J. Fluid Mech. (1998), *vol.* 366, *pp.* 159–177. Printed in the United Kingdom

Experimental study of interfacial solitary waves

By H. MICHALLET† AND E. BARTHÉLEMY

Laboratoire des Ecoulements Géophysiques et Industriels,
BP53, 38041 Grenoble Cedex 9, France

(Received 25 March 1997 and in revised form 21 January 1998)

A small-scale experiment was conducted (in a 3 m long flume) to study interfacial long-waves in a two-immiscible-fluid system (water and petrol were used). Experiments and nonlinear theories are compared in terms of wave profiles, phase velocity and mainly frequency–amplitude relationships. As expected, the KdV solitary waves match the experiments for small-amplitude waves for all layer thickness ratios. The characteristics of 'large'-amplitude waves (that is when the crest is close to the critical level – approximately located at mid-depth) asymptotically tend to be predicted by a 'KdV-mKdV' equation containing both quadratic and cubic nonlinear terms. In addition a numerical solution of the complete Euler equations, based on Fourier series expansions, is devised to describe solitary waves of intermediate amplitude. In all cases, solitary interfacial waves in this numerical theory tally with the experimental data. When the layer thicknesses are almost equal (ratio of lower layer to total depth equal to 0.4 or 0.63) both the KdV-mKdV and the numerical solutions match the experimental points.

1. Introduction

Oceanographers have observed internal solitary waves in many regions around the worlds oceans especially in straits, on continental margins and coastal zones. For a review of these investigations the reader is referred to Ostrovsky & Stepanyants (1989). Most of the observed solitons propagate at the interface between the thermocline and the deep sea. They are mainly excited by tidal flows over bottom topography (Goryachkin, Ivanov & Pelinovsky 1992; Lamb 1994; Gerkema & Zimmerman 1994). In lakes, such waves are thought to be generated in response to a strong wind event (Farmer 1978; Stevens *et al.* 1996). They contribute to the vertical mixing, while propagating at the interface, where a shear layer develops. The shoreward propagating waves eventually break in coastal zones where they are thought to be responsible for nutrient mixing (Sandstrom & Elliott 1984; Imberger 1995). They are also visible on airborne Radar images (Fu & Holt 1982; Alpers & Salusti 1983; Watson & Robinson 1991). Very recently, Brandt *et al.* (1997) have developed a rotationless Boussinesq-like model for the generation and propagation of internal waves (Diebels, Schuster & Hutter 1994 earlier devised a similar model, while Bauer, Diebels & Hutter 1994 included rotation in this type of model). We note that large solitary waves which are in good agreement with Synthetic Aperture Radar images of the Strait of Messina are simulated. Large-amplitude internal waves are frequently observed at sea. For instance, Kuznetsov, Paramonov & Stepanyants (1984) recorded an 80 m amplitude

† On leave at the Centre for Water Research, University of Western Australia, Nedlands 6907 Australia.

internal wave in the equatorial Atlantic Ocean (see also the investigations of Apel *et al.* 1985 in the Sulu Sea).

Our overall aim in this study is to assess different theories and models of long interfacial wave propagation. The KdV model holds for $h_0/\lambda \ll 1$ and $h/h_0 = O(1)$ (where h and h_0 are respectively the lower and upper layer thickness and λ is a characteristic wavelength). The KdV model is usually understood as a balance between nonlinearities and non-hydrostatic dispersion that produces waves of permanent form. More precisely the scaling required for these waves is

$$\frac{a}{h_0} = O\left(\frac{{h_0}^2}{\lambda^2}\right), \tag{1.1}$$

where a is the amplitude of the internal wave. Brandt *et al.* (1997) compared the solitary wave characteristics of a Boussinesq-like numerical model with KdV solitons. They show that for large amplitudes, that is for waves not complying with scaling (1.1), KdV theory is not adequate. In contrast Miyata's equation, designed to characterize them, matches the Boussinesq waves (Miyata 1988) to a much better extent than a second-order KdV equation. Miyata's equation is of a similar nature to the equations derived by Long (1956); it includes both quadratic and cubic nonlinearities but also a wealth of other higher-order nonlinear and dispersive terms (see its formulation recalled in the Appendix). Miyata (1988) based this new nonlinear equation on the assumption that $(h_0/\lambda)^4 \ll 1$ with no specification for the amplitudes. The same assumption in surface wave theory leads to equations (1.30)–(1.32) in Mei's book (1989, p. 509). Stationary interfacial solitary wave solutions of Miyata's equation are expressed implicitly with integrals. This implicit relation is computed numerically to give solitary wave profiles which are in good agreement with five experimental profiles. Unfortunately, too few experimental results are presented in his paper to reach any conclusion on the validity range of Miyata's equation.

Theoretical papers are far more numerous than experimental studies on the subject. Lee & Beardsley (1974), Segur & Hammack (1982), Kao, Pan & Renouard (1985), Helfrich & Melville (1986) and Maurer, Hutter & Diebels (1996) studied internal waves in a continuously stratified fluid composed of brine and water. Experiments with continuously stratified fluid involve mixing and interface thickening – drawbacks avoided with non-miscible fluids. Apart from the seminal study by Keulegan (1953), experimental works, such as those of Walker (1973) and Koop & Butler (1981) were performed for interfacial solitary waves in a two-fluid medium, which is the choice we made. Two-layer systems allow straightforward comparison with simple analytical results. A convenient way to compare experimental data to theoretical predictions is to utilize lengthscale–amplitude relationships. This kind of comparison is extensively developed by Koop & Butler (1981). Indeed to investigate the range of validity and accuracy of the KdV, B–O (Benjamin 1967 and Ono 1975), and 'finite depth' (Kubota, Ko & Dobbs 1978) equations they experimentally estimated an integral lengthscale (hereinafter called 'wavelength') related to the mass of the wave (figure 1) by computing

$$\lambda = \frac{1}{2a}\int_{-\infty}^{\infty} \eta(x)\, \mathrm{d}x, \tag{1.2}$$

where $\eta(x)$ is the interface displacement and x the horizontal coordinate. This is compared to the theoretical value for a given amplitude. The mass has a theoretical importance since it is an invariant of many nonlinear wave propagation models such as the KdV equation.

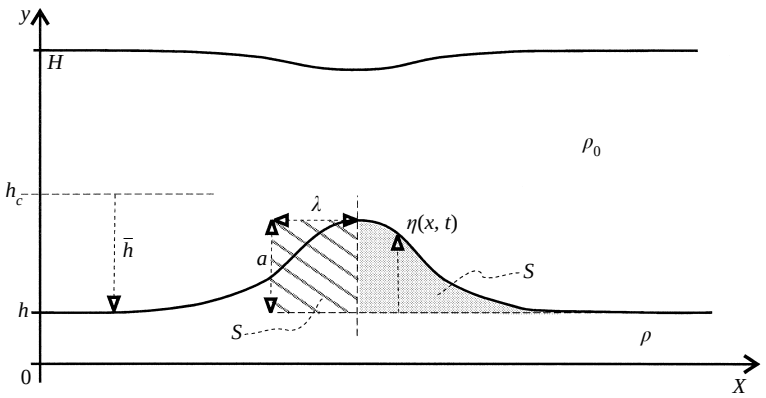

FIGURE 1. Schematic diagram and notation: $\lambda = S/a = (1/2a)\int_{-\infty}^{\infty} \eta(x)\,\mathrm{d}x$; $\bar{h} = h - h_c$; $y = 0$ is the horizontal bottom.

The cited experimental papers call for the following comments. First, these studies deal essentially with small-amplitude waves (amplitude over total depth: $a/H < 0.1$ where $H = h + h_0$). They all conclude that the first-order KdV equation is a very good description of their experimental data. However, Koop & Butler (1981) noted a discrepancy for larger amplitudes ($a/H > 0.05$). They therefore derive a KdV second-order equation, which was also obtained for continuously stratified fluids by Lee & Beardsley (1974), and which slightly improves the matching. Even though the second-order KdV equation combines quadratic nonlinear terms with cubic ones, it is still based on the scaling assumption (1.1). Secondly, the aforementioned experimental analyses investigate waves propagating in media with one layer thinner than the other (thinnest layer thickness to total depth less than 0.2). One recent exception is reported in the paper by Wessels & Hutter (1996), who discuss measurements of long internal waves (in a continuously stratified medium) for layer thickness ratios of 1/4 and 3/4. They describe the interaction of long internal waves with a sill. They consider the energy balance between transmitted and reflected waves. Nevertheless, they do not compare either the wavelength or frequency of these waves with the existing theoretical relations. Herein lies one of the specific motivations for this paper: to investigate experimentally the characteristics of interfacial solitary waves for a wide range of layer thickness ratios. Another recent exception is the investigation by Michallet & Barthélemy (1997). That study is restricted to the rigid lid case and three different thickness ratios. However, the paper mainly considers the experimental technique and data processing which provide experimental results which are used to demonstrate the relevance of this approach. Equivalent layer thickness cases (as $h/H = 0.4$ or 0.63) are not investigated, and we do that in the present paper.

In some shallow basins (Halpern 1971), as in some locations in the ocean (such as the Strait of Gibraltar, Watson & Robinson 1991) the interface is found to be close to the critical depth h_c (equation (2.7)). For an interface located at this critical level the KdV theory predicts no solitary wave since the nonlinear term vanishes (Long 1956). For mild stratifications this critical level is roughly half the total depth, that is h/H is close to 1/2. Kakutani & Yamasaki (1978) define asymptotic series with an expansion parameter a/H of the order of $(\bar{h}/H)$, where $\bar{h}$ is the distance between the interface and the critical level. Therefore, this new theory models

long waves propagating on an interface close to the critical level. It is generally admited that this expansion parameter has to be small, consequently the theory should only allow for weakly nonlinear waves. The new model equation (hereafter referred to as KdV-mKdV) resembles KdV with an extra cubic nonlinear term. It reads

$$\eta_t + (c + \alpha_0\eta - \alpha_1\eta^2)\eta_x + \beta\eta_{xxx} = 0. \tag{1.3}$$

If $\alpha_1 = 0$, (1.3) is the KdV equation. For $h = h_c$, $\alpha_0 = 0$. In such cases the equation is still nonlinear but then the balance is between dispersion and cubic nonlinearity. Details of the derivation of (1.3) and the expressions for the coefficients are found mainly in the works cited in § 2 and reconsidered in Michallet (1995). Benney & Ko (1978) also derived a KdV-mKdV equation for long large-amplitude waves in stratified fluids. An equation of type (1.3), also including dissipation, was derived by Helfrich & Melville (1986) to model internal solitary wave shoaling on slowly varying topographies. Numerical integrations of this equation (called 'EKdV' for extended KdV, see also Helfrich & Melville 1990) are in very good agreement in terms of wave profiles with experimental results (Helfrich & Melville 1986). While shoaling, waves may encounter parametric conditions for which the cubic nonlinear term dominates the quadratic one. The behaviour about the turning point $h = h_c$, for which the quadratic nonlinear term vanishes, was also investigated numerically by Helfrich, Melville & Miles (1984). However, these studies did not focus on the parametric range of validity of the EKdV equation.

Funakoshi & Oikawa (1986) showed numerically that for strong stratification ($\rho/\rho_0 = 3$; where ρ and ρ_0 are the densities of the lower and upper layers) and for cases where $h \sim h_c$ KdV-mKdV theory tallies with their numerical solution. They compared the mass of waves solutions of the Euler equations with the mass of solitary waves solutions of KdV-mKdV equations for various amplitudes. For the single stratification chosen, their computations indicate that large-amplitude solitary waves propagating on interfaces not too close to the critical level also match the mass–amplitude relationship of the KdV-mKdV equation. This is a puzzling conclusion. Indeed asymptotic theories are expected to hold only for small values of the expansion parameter. From this stems another motivation of our study. We wish to investigate for mild stratifications the behaviour of waves propagating on interfaces far from the critical level and amplitudes spanning the distance between the interface level and half of the total depth: such solitary waves will be designated 'large'-amplitude solitary waves. Michallet & Barthélemy (1997) have already pointed out the fact that the measured solitary waves are of the KdV type for small amplitudes and larger waves tend to verify a KdV-mKdV relationship. One of these 'large' internal solitary waves was observed by Sandstrom & Elliott (1984) on the Scotian Shelf: a solitary wave of approximately 53 m amplitude in a total depth of 160 m, with the mid-thermocline level located at 50 m below the sea surface. In this configuration, an equation of KdV-mKdV type (Kakutani & Yamasaki 1978; Miles 1981) is probably appropriate to predict large-amplitude solitary waves, as also suggested by Ostrovsky & Stepanyants (1989).

The paper is organized in the following manner. Section 2 describes the theoretical background for understanding nonlinear waves along with a brief literature review. Section 3 is devoted to a short description of the flume, the two-layer system, the ultrasonic probes and the data processing. Finally, in § 4, results are given for wave profiles, phase velocities and the amplitude–frequency relation of solitary interfacial waves ranging from small to large amplitudes.

2. Summary of previous theoretical results

2.1. *The KdV solution*

It is well known that the 'KdV' equation (an extension to two-layer systems of the study by Korteweg & de Vries 1895, see e.g. Benney 1966; Miles 1979) is a relevant approximation to describe solitary internal waves of small amplitude compared to the total depth (see e.g. Koop & Butler 1981; Kao *et al.* 1985).

We recall the main results for a two-fluid system, which corresponds to our experimental conditions. The notation is summarized on figure 1: h and H are the interface and surface levels at rest; ρ and ρ_0 are the lower and upper layer densities. An interface displacement $\eta(x,t)$ ruled by the KdV equation, possesses a solitary wave solution expressed by

$$\eta(x,t) = a\ \mathrm{sech}^2\left[\frac{x - C_k t}{\lambda_k}\right], \tag{2.1}$$

where a and C_k are the amplitude and the phase velocity. The solitary wave steadily propagates at constant phase speed C_k; λ_k in (2.1) is the characteristic length of the solitary wave and is equal to λ defined by (1.2) (Koop & Butler 1981; see figure 1). In the framework of the KdV theory with a free surface boundary condition, C_k and λ_k are related to the layer thicknesses and densities as follows (the equations with the rigid lid assumption may be found in Michallet & Barthélemy 1997):

$$C_k = C_0 + a\,\frac{C_0}{2h}\,\frac{\rho/\rho_0 - h^2(H-h)/(H'-h)^3}{\rho/\rho_0 + h(H-h)/(H'-h)^2} \tag{2.2}$$

with

$${C_0}^2 = \frac{gH}{2}\left[1 - \left(1 + \frac{4h(h-H)(\rho-\rho_0)}{\rho H^2}\right)^{1/2}\right], \tag{2.3}$$

$$\lambda_k = \left(\frac{1}{a}\,\frac{4h^3}{3}\,\frac{\rho/\rho_0 + (H'-h)/h + (H-H')^3/\left[h(H'-h)^2\right]}{\rho/\rho_0 - h^2(H-h)/(H'-h)^3}\right)^{1/2} \tag{2.4}$$

and

$$H' = H - \frac{{C_0}^2}{g}. \tag{2.5}$$

(Note that $H' = H$ for the rigid lid case.) The frequency ω_k is preferred for comparison with the experiments, since the data consist of recordings of interface displacement $\eta(x,t)$ at one location against time. The integral frequency scale ω_k is defined by

$$\omega_k = \frac{2a}{\displaystyle\int_{-\infty}^{\infty} \eta(t,x_0)\ \mathrm{d}t} = \frac{C_k}{\lambda_k}; \tag{2.6}$$

λ_k in (2.4) is not defined for the specific value $h = h_c$, where h_c is defined by (Kakutani & Yamasaki 1978)

$$\frac{{h_c}^2(H-h_c)}{(H'-h_c)^3} = \frac{\rho}{\rho_0}. \tag{2.7}$$

If $h = h_c$ zero-amplitude solitary waves are the only solutions of KdV theory allowed. Note that the polarity of the solitary wave is ruled by the position of the interface with respect to the critical level h_c: when the interface is below (above) h_c the solitary wave is of elevation (of depression). This behaviour is recognized to be supplied by

the complete Euler equations (Craig & Sternberg 1991). This means, for instance, that an interface disturbance which crosses the critical level h_c cannot be of permanent type propagating steadily at constant velocity (Koop & Butler 1981).

2.2. *The KdV-mKdV solution*

The KdV-mKdV nonlinear equation (Miles 1981; Funakoshi 1985; Funakoshi & Oikawa 1986) predicts solitary waves of amplitude a ranging from 0 to $\bar{h}$, where $\bar{h}$ is the distance between the interface and the critical level:

$$\bar{h} = h - h_c; \tag{2.8}$$

$\bar{h}$ is the limiting amplitude a_c of the wave. The main assumption in deriving this equation is to consider the wave amplitude to be of the same order as $\bar{h}$, which is also small compared to the total depth. The wave of the limiting amplitude a_c has an infinite mass (λ tends to infinity). An interfacial solitary wave whose interface elevation $\eta(x,t)$ is ruled by the KdV-mKdV equation also travels at constant speed without change of shape and is expressed by (other solitary waves of bore type also exist)

$$\eta(x,t) = a\,\frac{\operatorname{sech}^2\left[\kappa(x - C_m t)\right]}{1 - \mu\tanh^2\left[\kappa(x - C_m t)\right]}; \tag{2.9}$$

the expressions for μ, κ and C_m are (for a free upper boundary)

$$\left.\begin{array}{ll} \text{if } \bar{h} > 0: & \mu = h''/h', \\ \text{if } \bar{h} < 0: & \mu = h'/h'', \end{array}\right\} \tag{2.10}$$

$$\kappa = \left(-\frac{B}{A}h'h''\right)^{1/2} \tag{2.11}$$

with

$$A = \frac{2C_{0m}}{3H'}\left[\frac{H' - h_c}{H - h_c}\left[(H' - h_c)^3 + (H - H')^3\right] + {h_c}^3\right], \tag{2.12}$$

$$B = \frac{-C_{0m}}{2(h_c - H')^2}, \tag{2.13}$$

$$h' = -\frac{\beta}{\alpha}\bar{h} - \frac{1}{\alpha}[(C_m - C_{0m})/B + (\beta^2 - \alpha)\bar{h}^2]^{1/2}, \tag{2.14}$$

$$h'' = -\frac{\beta}{\alpha}\bar{h} + \frac{1}{\alpha}[(C_m - C_{0m})/B + (\beta^2 - \alpha)\bar{h}^2]^{1/2}, \tag{2.15}$$

$$\alpha = 1 + \frac{5}{4}\,\frac{H - H'}{H'}, \tag{2.16}$$

$$\beta = 1 + \frac{1}{2}\,\frac{H - H'}{H'}, \tag{2.17}$$

$$C_m = C_{0m} + B\left[(\alpha\, a + \beta\, \bar{h})^2 - (\beta^2 - \alpha)\bar{h}^2\right], \tag{2.18}$$

where H' and h_c are defined as in (2.5) and (2.7); C_{0m} is defined by equation (2.3) with $h = h_c$.

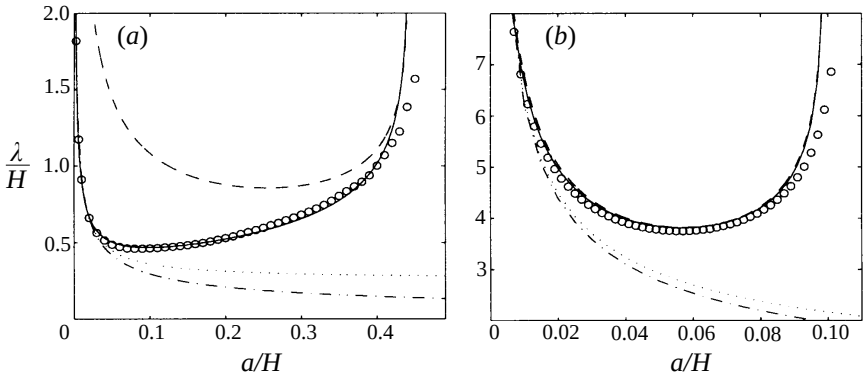

FIGURE 2. Dimensionless integral lengthscale λ (1.2) of solitary waves versus their dimensionless amplitude. All the curves plotted are theoretical predictions. Rigid lid case for $\rho_0/\rho = 0.78$: numerical results (○); analytical curves KdV first-order (–·–), KdV second-order (Koop & Butler 1981) (···), KdV-mKdV (––) and Miyata (—). (*a*) $h/H = 0.09$, $L/H \sim 80$; (*b*) $h/H = 0.63$, $L/H \sim 350$.

The polarity of the solitary waves is ruled by the sign of $\bar{h}$, i.e. $a \lessgtr 0$ for $\bar{h} \gtrless 0$. A ω_m equivalent to (2.6) is computed for large-amplitude waves:

$$\omega_m = \frac{2a}{\displaystyle\int_{-\infty}^{\infty} \eta(t, x_0)\, \mathrm{d}t} = \frac{C_m\, \kappa\, \mu^{1/2}}{\operatorname{arctanh} \mu^{1/2}}. \tag{2.19}$$

2.3. *Numerical solutions*

Both KdV and KdV-mKdV equations possess periodic wave solutions ('cnoidal waves'). When their wavelength tends towards infinity, these waves tend towards solitary wave solutions. The foundation of the numerical approach, first described by Funakoshi & Oikawa (1986), is to consider periodic waves 'exactly' fulfilling (in a numerical sense) the Euler equations. The unknowns are written as Fourier series. The numerical procedure applies to truncated series. The method is reported by Holyer (1979) for interfacial waves, and Rienecker & Fenton (1981) for progressive surface waves. A very large value is chosen for the wavelength L of the computed waves: L is more than 80 times H. These very long waves are akin to solitary waves. The length L of the computational box is also chosen in relation with our experimental set-up. Indeed the numerics compare well to the experimental results since our flume length is roughly 30 times H.

We generalize the method of Funakoshi & Oikawa (1986) to take into account free surface conditions. Two equations are obtained at the surface instead of one. The surface displacement is also written as a truncated Fourier series. The five relations written at $N = 160$ collocation points yield a system of $(5N + 2)$ nonlinear equations (instead of $(3N + 1)$ equations on $N = 200$ points for the rigid lid case).

An iterative Newton–Raphson scheme is employed to solve the system. For each depth ratio, the initial small-amplitude guess is a linear sinusoidal wave of very small amplitude ($a/H = 10^{-4}$) for the rigid lid configuration. The solution computed at the next step from this guess with the complete nonlinear equations is of a slightly larger amplitude. The resulting solution provides the guess for the next iterative process and so forth until the near limiting amplitude.

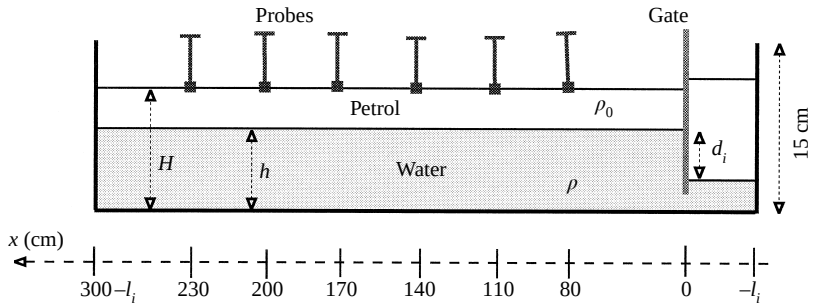

FIGURE 3. Schematic diagram of the experimental set-up; the length of the flume is 3 m and the width 10 cm; the interface level h ranges from 1 to 9 cm approximately with total depth $H \sim 10$ cm; density ratio $\rho_0/\rho = 0.78$. An initial condition for generating a solitary interfacial wave is also represented.

2.4. *Theoretical comparisons*

This theoretical part is concluded by presenting on figure 2 the main characteristics of interfacial waves as given by the models and theories. On both figures 2(*a*) and 2(*b*) the numerical solutions and Miyata's model can be seen to be in agreement with the KdV model in the small-amplitude range. On the other hand they match the KdV-mKdV model for very large waves. Note that KdV-mKdV and Miyata's relations predict the same limiting amplitude value, for which the mass (and thus the wavelength) tends towards infinity. The curve corresponding to the numerical computation merges with Miyata's solutions, except near this limiting amplitude. Numerical convergence is then hard to obtain, because of the approaching theoretical singularity. λ probably becomes too large to consider the cnoidal solution as a soliton (for say $\lambda > L/70$).

Predictions of the KdV second-order theory (Koop & Butler 1981) are also plotted. The curve (dotted line) lies between KdV and Miyata's curves. However it monotonically follows the KdV first-order scaling. It appears that the improvement over the KdV first-order scaling is small if we regard the numerical predictions as exact. Therefore, it is felt that the KdV second-order equation is unable to achieve as good a description of solitary waves of large amplitudes as the KdV-mKdV equation might do. Moreover figure 2 also shows that the validity range of the KdV second-order theory is of equivalent extent. Consequently we will not plot the KdV second-order scalings when comparing the models with the experimental results in § 4.

The important conclusion is: Miyata's solitary wave solution is identical to the numerical solution for the layer thickness ratios considered. For an interface close to the critical level ($h/H = 0.63$: figure 2*b*), KdV-mKdV, Miyata's curves and the numerical data obtained by the method of Funakoshi & Oikawa (1986) merge together. All these general new features will be discussed in § 4 by comparison with the experimental data.

3. Facility and experimental procedure

The experimental set-up, including the probing device and the data processing, have been extensively discussed in Michallet & Barthélemy (1997). The main points are recalled here. The wave flume, schematically drawn on figure 3, is approximately 3 m long and has a 15 cm $\times$ 10 cm cross-section. Over the total flume length the bottom is horizontal with an average error of 0.01 cm. No absorbing device was

installed. Waves reflect off the vertical wall at the downstream end of the flume. The two fluids chosen are immiscible liquids having different specific gravities, respectively petrol product 'Exxsol D60' (density $\rho_0 = 0.78$ kg l^{-1}, viscosity $\nu = 1.64$ m^2 l^{-1}) and water ($\rho = 1$ kg l^{-1}). Walker (1973) used a two-fluid system with comparable physical characteristics. As noted before, two-fluid systems are convenient to use: no mixing occurs at the interface, which is thus always well defined.

Interfacial long waves are generated using a gate-type wave-maker, similar to that described by Kao *et al.* (1985). A watertight, manually movable gate is located vertically near the upstream end of the tank (see figure 3). The interface level behind the gate is modified so as to be different from that of the main part of the flume by any desired amount. The gate is lifted to allow the step-like condition to evolve downstream into waves. The wave-generation system actually has two degrees of freedom: the height d_i and the length l_i of the step-like condition. A difference d_s in surface levels between each side of the gate, proportional to the difference d_i in interface levels (figure 3) is generated:

$$d_s \sim -\frac{\rho - \rho_0}{2\rho_0}\, d_i \sim -0.14\, d_i.$$

Experimentally this difference creates barotropic waves. It is worth noting that the height of the resulting fast mode is much smaller than in a piston-like generating system, such as those used by Walker (1973) or Segur & Hammack (1982). The gate is not completely lifted out of the petrol but stopped just below the free surface. Practice has also shown that a 'smooth' and 'slow' removal is preferable to a 'rough' one to minimize the generation of barotropic disturbances. They are, nevertheless, noticeable on figure 4(*b*) for $t < 10$ s. Note that when the thinnest layer is on the top ($h/H > 0.5$) these barotropic disturbances are slightly greater but yet negligible compared to the baroclinic waves. Consequently, we never felt it necessary to filter these waves out. Nonetheless, our fitting technique described below probably removes some of the barotropic signatures. Moreover, on the downstream side of the gate, the flume could be totally covered by a rigid lid, avoiding the propagation of the fast mode.

Some authors reporting experiments with a free surface upper boundary made the assumption when analysing the data that this upper boundary can be considered as rigid (see e.g. Koop & Butler 1981; Kao *et al.* 1985). This approximation is satisfactory, but only in the case of a small difference in densities ($\rho - \rho_0 \sim 1\%$): the resulting internal solitary wave is then approximately independent of whether the upper boundary is rigid or free (Keulegan 1953). But in our experiments, the density difference is rather large ($\rho - \rho_0 = 22\%$): to consider the free surface as a rigid lid is inaccurate. Indeed the computation of h_c (2.7) depends on the upper boundary condition. When $\rho_0/\rho = 0.99$, $h_c/H = 0.501$ with the rigid lid assumption, and $h_c/H = 0.499$ for a free surface. But if $\rho_0/\rho = 0.78$, $h_c/H = 0.531$ and 0.486, respectively.

Six ultrasonic probes were located along the centre of the flume. The outputs are recorded simultaneously on a PC. The raw signal is processed by fitting the experimental points with a function calculated by a least-square method (Michallet & Barthélemy 1997). The fitting function is of the form

$$F = a_0 + a_2 \left(1 - \tanh^2 \left[\omega\, (t - t_0)\right]\right), \tag{3.1}$$

where a_0 (mean level of the interface after the initial condition for the solitary wave is created), t_0 (time at which the wave maximum is recorded), a_2 (wave amplitude) and ω

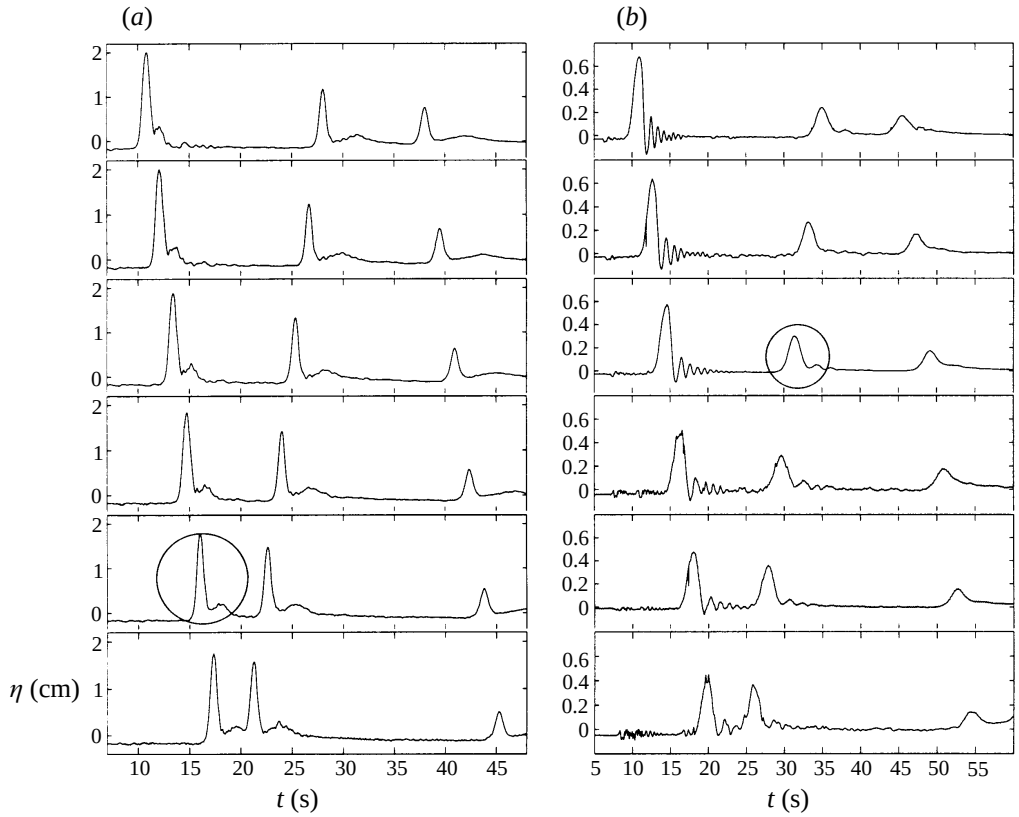

FIGURE 4. Time series at six locations of interface displacement (η) after generation and reflection of interfacial waves (free surface condition). The encircled areas are enlarged on figure 6. (*a*) The main pulse is very close to a solitary wave; thickness ratio $h/H = 0.20$ with $H = 10.04$ cm. Distances of probes from wave-maker (from top to bottom): $d = 90$, 120, 150, 180, 210, 240 cm. (*b*) The leading pulse before reflection points to a non-permanent wave, while after reflection it acquires a symmetric solitary wave-like profile; $h/H \sim 0.40$ with $H \sim 5.4$ cm. $d = 80$, 110, 140, 170, 200 and 230 cm (from top to bottom).

(characteristic frequency) are the unknown numerical values computed by the fitting process. The quadratic error between (3.1) and the signal is minimized. Formula (3.1) is fitted mainly on the front part of the wave. This front part is not disturbed by the dispersive train or a possible smaller soliton always trailing behind. The pulse shape given by (3.1) is of the same kind as the wave profiles obtained in (2.1) and (2.9), but in the theoretical equations the frequency is linked with the amplitude, densities and layer thicknesses (2.6), (2.19) while for (3.1), a_0, t_0, a_2 and ω are independent numerical values deduced from the experimental signals. The processed experimental values of a_2 and ω are thus obtained. The latter is compared to the analytical values given by (2.6) and (2.19). This data processing procedure filters noise but also, as mentioned above, a fraction of the barotropic signatures on the interface while preserving the nonlinear features of the waves. It provides an automatic data elimination scheme by which pulses too perturbed by barotropic waves or other sources are not analysed (Michallet & Barthélemy 1997).

The phase velocity C is estimated in a different way, from the outputs of two consecutive probes. This value is thus deduced from the distance separating the two

h/H	Upper condition	h (cm)	H (cm)	$a_c = \lvert\bar{h}\rvert$ (cm)	a/H	a/a_c
0.09	Rigid lid	0.92	10.24	4.52	0.02–0.12	0.045–0.27
0.19†	Rigid lid	1.95	10.24	3.49	0.01–0.22	0.03–0.65
0.20	Free surface	2.02	10.02	2.85	0.01–0.225	0.035–0.79
0.29†	Rigid lid	2.97	10.24	2.47	0.01–0.11	0.04–0.46
0.40‡	Free surface	2.15	5.42	0.48	0.01–0.07	0.11–0.78
0.63‡	Rigid lid	3.12	4.98	0.48	0.04–0.07	0.42–0.73
0.77	Free surface	4.37	5.66	1.62	0.02–0.23	0.07–0.88
0.84	Rigid lid	8.59	10.22	3.16	0.01–0.22	0.03–0.71
0.91	Free surface	7.28	8.00	3.39	0.005–0.19	0.01–0.45
0.96†	Rigid lid	12.94	13.48	5.78	0.002–0.15	0.005–0.35

TABLE 1. Summary of experimental conditions: h and H are the interface and surface levels at rest, $\bar{h}$ is the difference between h and the critical level h_c, a_c is the limiting amplitude defined by the KdV-mKdV theory. Also presented are the ranges of amplitude a of the measured solitary waves. For all runs the density ratio is $\rho_0/\rho = 0.78$. Data noted † were presented in Michallet & Barthélemy (1997); ‡ concern reflected waves only.

probes and the times at which the maxima of the two corresponding signals pass them. The amplitudes of the two pulses are not equal. Therefore, the estimation of C is ascribed to a wave of average amplitude. Note that the solitary wave is shifted during its interaction with the wall (see e.g. Maurer *et al.* 1996). Therefore the phase velocity is never estimated with two pulses of the same wave separated by a reflection. Moreover the probes are located far enough from the reflecting walls (at least 30 cm away) so that any instabilities or transient motions which might be created during the interaction do not alter the wave when it is measured.

The experimental errors in the data provided by the processing techniques are the following: 8 % (about 0.06 cm) on the amplitude a_2; 11 % (about 0.4 s^{-1}) on the frequency ω; 9 % (about 1.6 cm s^{-1}) on the phase velocity C. These estimations were obtained by comparing the simultaneous outputs of probes located at the same distance from the gate. These estimations allow error bars to be plotted. These bars indicate the errors due to sampling and processing techniques. More details on error estimations are found in Michallet & Barthélemy (1997).

4. Comparison with experiments

Series of long waves were generated at the interface of the two-layer system. The parameters of these experiments are summarized in table 1. The probes are located along the flume in order to examine the propagation of the solitary wave. Each wave is recorded as it travels three times along the flume (waves can be recorded and processed once they are reflected). The recordings of two different runs are reproduced on figure 4.

On figure 4(*a*) for which $h/H = 0.20$ (a thin layer case), the leading solitary wave is followed by a second smaller wave. It is probably a smaller soliton which propagates more slowly. In fact the time interval between two maxima increases with time t. On the first probe ($d = 90$ cm) it measures 1.3 s before reflection (graph at the top of figure 4*a*). On the same probe but after one reflection (the waves have then travelled 476 cm) the time lapse is 3.1 s. The frequency–amplitude relationship of the leading solitary wave as it passes each probe is plotted on figure 5(*a*). We recall that the

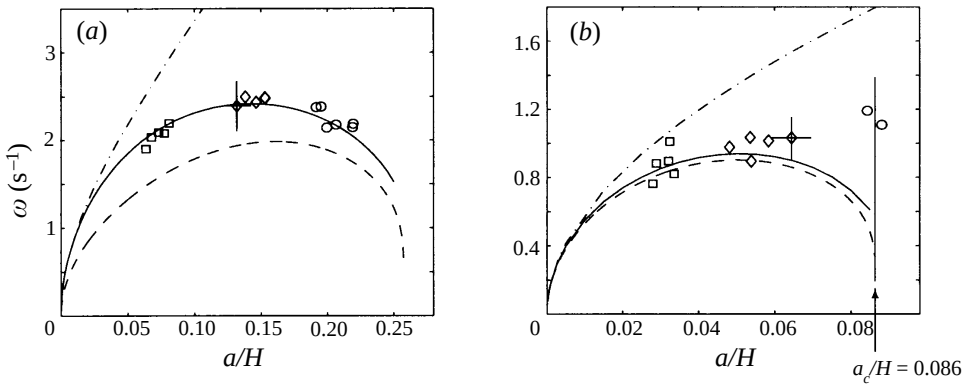

FIGURE 5. Characteristic wave frequency ω of the runs of figures 4(a) and 4(b): incident (○), once (◇) and twice (□) reflected waves; analytical curves: KdV first-order (– · –) and KdV-mKdV (– –); numerical curve (—). (a) $h/H = 0.20$; H=10.04 cm. (b) $h/H = 0.40$; H=5.4 cm. a_c is the limiting amplitude of the KdV-mKdV theory.

frequency scale such as (2.6) is preferred to the integral lengthscale (1.2). Computing (1.2) from the data also involves deducing the phase velocity from the data; the error on (1.2) is therefore larger since the error on the phase velocity has to be added to the error on the frequency. On figure 5(a), the group of points of larger amplitudes corresponds to the incident wave, the group of four points in the middle corresponds to the wave after one reflection and the group on the left corresponds to the twice reflected wave. The damping of the wave during its propagation is significant. The wave actually loses about 3% of its amplitude after travelling 30 cm between two probes. This damping rate is of the same order as the one measured by Koop & Butler (1981). Numerous studies (e.g. Leone, Segur & Hammack 1982; Helfrich & Melville 1986) have shown a qualitative agreement between laboratory measurements and models assuming slow adiabatic changes in wave properties. But it is not the purpose here to study such dissipation (see also Maurer *et al.* 1996 for such a study). Indeed on figure 5(a), all points merge with the numerical curve for which viscous effects are neglected: whatever the dissipation, the frequency–amplitude relation is fulfilled at every stage of wave propagation. Accordingly the balance between dispersive and nonlinear effects is not affected by viscous ones still acting, we suggest, at much bigger timescales.

Important conclusions are drawn from this plot. For small amplitudes ($a/H < 0.1$) the experimental points are not very far off the KdV curve, the data are close to the numerical curve for the entire amplitude range and seem to tend towards the KdV-mKdV curve for the larger amplitudes. The profile corresponding to one of the largest-amplitude points (to the right on figure 5a) is shown magnified on figure 6(a). This leading solitary wave profile corresponds to the encircled zone of figure 4(a). This experimental profile is compared to the theoretical profiles (KdV, KdV-mKdV and numerical) of the same amplitude. The front side of the wave is unperturbed and merges perfectly with the numerical profile, although the back side is slightly modified by the trailing smaller soliton. Figure 6(a) is a meaningful example of the general feature of most solitary waves measured: the KdV profile is narrower than the experimental one, which is itself narrower than the KdV-mKdV profile. Figure 7(a) shows the dimensionless phase velocity $C/(gH)^{1/2}$ against the dimensionless amplitude a/H for experimental conditions identical to those of

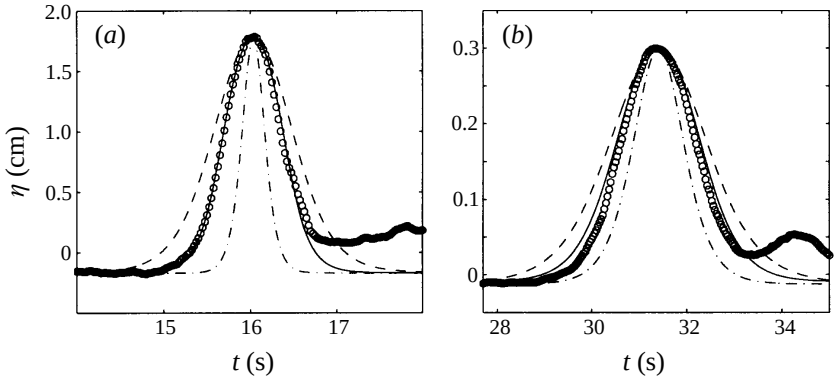

FIGURE 6. Interface displacement (see figure 4): experimental data (○), numerical profile (—), KdV first-order (– · –) and KdV-mKdV (– –) profiles. (*a*) Incident leading pulse, $h/H = 0.20$; $H = 10.04$ cm and $d = 210$ cm. (*b*) Reflected leading pulse, $h/H = 0.40$; $H = 5.41$ cm and $d = 416$ cm.

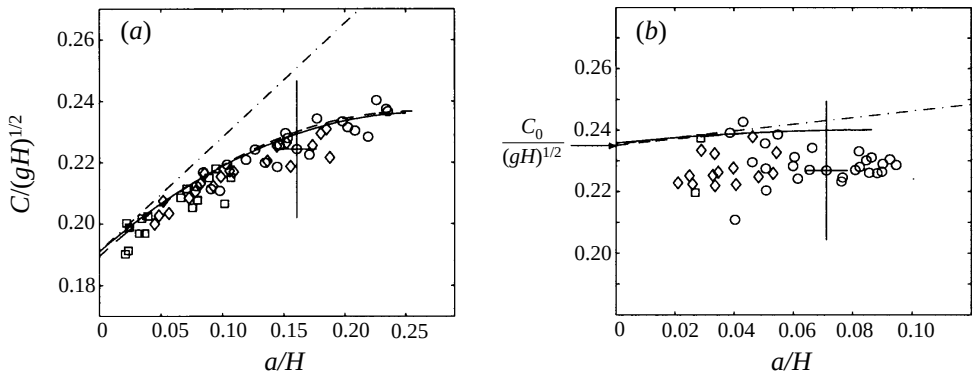

FIGURE 7. Dimensionless phase velocity of interfacial waves versus dimensionless amplitude. Incident (○), once (◇) and twice (□) reflected waves; analytical curves: KdV first-order (– · –) and KdV-mKdV (– –); numerical curve (—). (*a*) $h/H = 0.20$. (*b*) $h/H = 0.40$, C_0 is the linear long wave phase speed.

figure 5(*a*). The match between the experimental data and the numerical curve is very good. The KdV-mKdV predictions and the numerical curve are almost equal. Taking into account the scattering of the experimental points, it is therefore difficult to differentiate KdV-mKdV from the numerical solution, while this is possible for the frequency (figure 5*a*). On the corresponding frequency–amplitude plots the KdV-mKdV result is clearly different from the numerical solution with respect to the size of the error bars. This point was already mentioned by Koop & Butler (1981): the frequency–amplitude relationship is certainly a good criterion for testing theoretical predictions.

For $h/H = 0.4$ (an equivalent layer thickness case) we plot the interface displacements recorded on the six probes (figure 4*b*) and the corresponding plot of the frequency–amplitude relation (figure 5*b*). Note the big dispersive wave trailing the leading wave (for $t < 23$ s). The two circles (○) on figure 5(*b*) correspond to waves measured on the two probes nearest to the endwall. The four other incident waves (for $t < 17$ s) have been eliminated by the processing procedure because they were too far from being symmetric (see in Michallet & Barthélemy 1997 how the asymmetry is

quantified). One of these points is related to a wave of amplitude exceeding the critical amplitude a_c as predicted by the KdV-mKdV theory ($a_c/H = 0.086$ for this thickness ratio). This seems to be in contradiction with the KdV-mKdV theory. If this same leading wave is considered once it is reflected and is measured on the $d = 140$ cm plot, figure 6(*b*) shows that it has formed while propagating and dissipating into a symmetric wave that is well reproduced by the numerical profile. The dispersive wave trailing the soliton is now very weak (figure 4*b*). The phase velocity–amplitude relationship for this thickness ratio ($h/H = 0.40$) is shown on figure 7(*b*). The experimental values are systematically smaller than the long linear wave phase speed C_0 (defined by (2.3)). This shift is not very large: of the order of 5%, which is less than the error ascribed to each point. This was also a feature of some waves measured by Segur & Hammack (1982). They attributed this to viscous effects. Probably the hypothesis that dispersion and nonlinearities 'work' faster than dissipation may be a shortcoming in cases with thick layers. Nevertheless the frequency–amplitude relationship (figure 5*b*) seems to indicate that the waves are described by the KdV-mKdV model in a satisfactory way.

It is experimentally difficult to produce near-limiting-amplitude waves, particularly when the interface is near the critical level. The step-like initial condition, if not too small, breaks dramatically and the wave requires a long distance to become established. Indeed, for these types of layer thickness ratios, waves have a longer sorting distance (i.e. the travel distance required for a set of ordered solitons to evolve and separate from the initial disturbance, see Hammack & Segur 1974) than in a thin layer case (Pan 1984; Michallet 1995), mainly because all the waves are propagating at a similar phase velocity. It is essential to produce large initial conditions and to measure only the reflected waves in order to consider that they have travelled sufficiently to be symmetric in shape. Therefore only the points corresponding to reflected waves are plotted on figure 8(*a*). The experimental points are scattered and do not precisely match any theoretical curve. This scattering is certainly due to the fact that waves need long timescales to become established, as discussed above, but also to an additional error. This error is explained by the fact that the incident waves travel in a two-layer system of thickness ratio h/H, which differs from the h/H encountered by the reflected waves. Indeed the wave loses mass by dissipation, thus modifying h/H (this is noticeable on figure 4*b*). When the level at rest h is very close to the critical level h_c, a small variation of h/H induces a considerable difference in $h - h_c$, and thus a large shift in the theoretical curves, which are sensitive to this difference. With regard to this additional error, it may be concluded that the numerical and the KdV-mKdV analytical frequency–amplitude relations are a good approximation of the experimental data for $h/H = 0.40$.

Results for the frequency–amplitude relationship are presented for other thickness ratios $h/H = 0.63$, 0.77, 0.84, 0.91 and 0.09 on figure 8(*b–f*), respectively. Some are for a rigid lid condition ($h/H = 0.63$, 0.84 and 0.09), while the remaining ones are for a free surface configuration. The same trends as those described above are again found: the experimental points match the numerical curves, they asymptotically satisfy the KdV theory for solitary waves of small amplitude, while they asymptotically tend to conform to KdV-mKdV theory for the large amplitudes. The concept of 'large amplitude' is highlighted by all these examples. Indeed when the amplitude is more than 0.4 times the limiting amplitude a_c, the data comply more with the KdV-mKdV curve than with the KdV one. Otherwise when the level at rest is close to the critical level (for $h/H = 0.63$) the data, the KdV-mKdV curve and the numerical

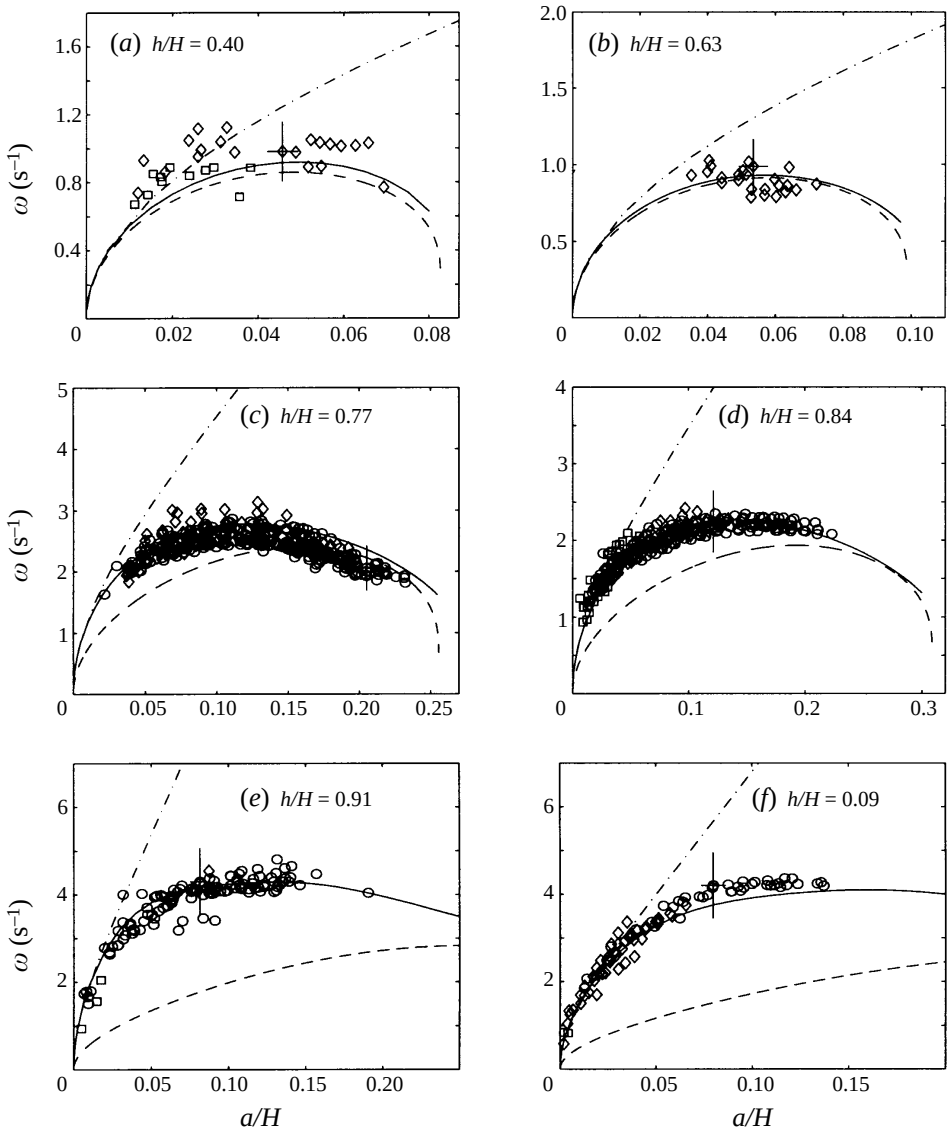

FIGURE 8. Characteristic frequency ω versus the dimensionless amplitude a/H: incident (○), once (◇) and twice (□) reflected waves; analytical curves: KdV first-order (–·–) and KdV-mKdV (––); numerical curve (—). (a, c, e) for a free surface condition; (b, d, f) for a rigid lid condition.

curve are very close over the entire amplitude range. The phase velocity is also plotted versus the amplitude on figure 9. For this thickness ratio ($h/H = 0.09$), the differences between the various theoretical curves are sufficiently large to allow a comparison with the experimental data. The behaviour described above concerning the frequency–amplitude relationship is again found: the waves verify KdV theory for small amplitudes ($a/H < 0.05$) and tend to verify KdV-mKdV theory for large amplitudes ($a/H > 0.1$).

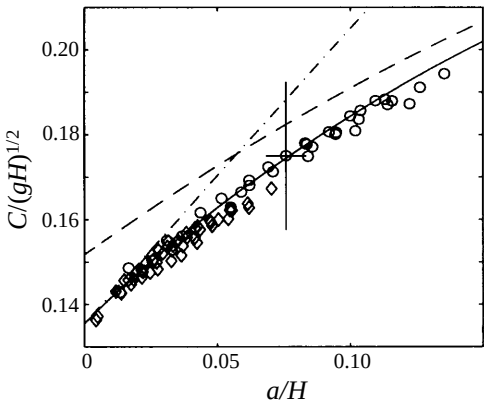

FIGURE 9. Phase velocity versus amplitude for $h/H = 0.09$; rigid lid condition; incident (○), once (◇) and twice (□) reflected waves; analytical curves: KdV first-order (– · –) and KdV-mKdV (– –); numerical curve (—).

5. Conclusions

Based on the theoretical comparisons of § 2, the following general observations may be made: (i) the numerical solution matches the KdV theory for small amplitudes; (ii) the numerical solution also correctly approximates the KdV-mKdV for large amplitudes; (iii) when the interface is close to the critical level h_c (say $0.4 \leqslant h/H \leqslant 0.63$) the numerical solution and KdV-mKdV theory are in good agreement; (iv) Miyata's equation (Miyata 1988) predicts solitary wave solutions that tally with the numerical solutions for a rigid lid assumption, and predicts the same limiting amplitude as the KdV-mKdV theory.

These conclusions have been assessed by comparing experimental data with the aforementioned models. The classical KdV equation provides wave characteristics that indeed fit with the characteristics of experimentally generated small-amplitude solitary waves ($0.01 < a/H < 0.05$) for all layer thickness ratios. This was already partially demonstrated in the rigid lid case in Michallet & Barthélemy (1997). New results concerning large-amplitude waves (that is wave heights of the order of the distance $\bar{h}$ separating the interface from the critical level) and the KdV-mKdV model are obtained. The experiments show that $\bar{h}$ is an important parameter in choosing the relevant model of nonlinear waves in two-fluid systems of finite depth. First, in cases where the interface is 'far' from h_c ($h/H < 0.4$ and $h/H > 0.63$) large-amplitude interfacial solitary waves show experimental frequency–amplitude relationships that tend to be predicted by KdV-mKdV equation (especially for $h/H \sim 0.2$ and $h/H \sim 0.8$). Secondly it has been established experimentally in the present paper that for $h/H = 0.4$ and $h/H = 0.63$ waves are of KdV-mKdV type for all amplitudes ($0.1 < a/\bar{h} < 0.8$) as predicted by Kakutani & Yamasaki (1978) although the data in these cases are more scattered than in the others. This was expected for it corresponds to the assumptions included by Kakutani & Yamasaki (1978) in the KdV-mKdV model. Finally, for the intermediate range of amplitude, only numerical integration of the full Euler equations achieves sufficient matching, and this is true for all depth ratios.

In addition experiments suggest that interface disturbances of amplitudes larger than a_c are too far from being symmetric to be considered as established and thus as solitary waves. Theoretical (Kakutani & Yamasaki 1978) and numerical

works (Funakoshi & Oikawa 1986; Turner & Vanden-Broeck 1988; Evans & Ford 1996) predict that the solitary wave has a broadening lengthscale for nearly limiting amplitudes. However, it was extremely difficult to generate such waves experimentally since there is considerable breaking during the generation process and other significant dissipative effects during propagation.

The first author is grateful to the French Ministry of Education (MESR), which supported this work. The authors would like to thank J.-M. Barnoud for his help in constructing the experimental facilities, and D. Auchère and J.-P. Barbier-Neyret for the improvement of the ultrasonic measuring device.

Appendix. The Miyata equation (Miyata 1985, 1988)

Consider a two-fluid system with the rigid lid assumption (using the same notation as in § 2). Both fluids are assumed to be incompressible and irrotational. The waves are assumed to be long:

$$\left(\frac{h+a}{\lambda}\right)^4 \ll 1 \quad \text{and} \quad \left(\frac{h_0}{\lambda}\right)^4 \ll 1 \tag{A 1}$$

if we consider that $h < h_0$. Note that the wave amplitude a may be larger than h, as long as (A 1) is satisfied. Introducing the new variables $\theta = (x - Ct)/h$ and $\eta' = \eta/h$, the following differential equation is obtained:

$$\frac{F^2 r^2 (1+rs)}{3(r+s)} \left(\frac{\mathrm{d}\eta'}{\mathrm{d}\theta}\right)^2 + \frac{E\eta'^2 + D\eta'^3 - \eta'^4}{1+G\eta'} = 0 \tag{A 2}$$

where

$$D = \frac{r^2 - s + r(F^2-1)(1-s)}{r+s}, \quad E = -r(F^2-1), \quad G = \frac{r^2 s - 1}{r(1+rs)},$$

$$r = \frac{h_0}{h}, \quad s = \frac{\rho_0}{\rho}, \quad F^2 = \frac{(r+s)C^2}{g(1-s)h_0} = \frac{(1+a/h)(1-a/h_0)}{1-(a/h)(1-s)/(r+s)}.$$

Equation (A 2) can be analytically solved in terms of incomplete elliptic integrals of the first and the third kind. Note that if the interface is close to the critical level (2.7), G tends toward zero and (A 2) becomes a KdV-mKdV equation.

REFERENCES

Alpers, W. & Salusti, E. 1983 Scylla and Charybdis observed from space. *J. Geophys. Res.* **88**, 1800–1808.

Apel, J. R., Holbrook, J. R., Liu, A. K. & Tsai, J. J. 1985 The Sulu Sea internal soliton experiment. *J. Phys. Oceanogr.* **15**, 1665–1651.

Bauer, G., Diebels, S. & Hutter, K. 1994 Nonlinear internal waves in ideal rotating basins. *Geophys. Astrophys. Fluid Dyn.* **78**, 21–46.

Benjamin, T. B. 1967 Internal waves of permanent form in fluids of great depths. *J. Fluid Mech.* **29**, 559–592.

Benney, D. J. 1966 Long non-linear waves in fluid flows. *J. Maths & Phys.* **45**, 52–63.

Benney, D. J. & Ko, D. R. S. 1978 The propagation of long large amplitude internal waves. *Stud. Appl. Maths* **59**, 187–199.

Brandt, P., Rubino, A., Alpers, W. & Backhaus, J. O. 1997 Internal waves in the Strait of Messina studied by a numerical model and Synthetic Aperture Radar images from the ERS 1/2 satellites. *J. Phys. Oceanogr.* **27**, 648–663.

Craig, W. & Sternberg, P. 1991 Comparison principles for free-surface flows with gravity. *J. Fluid Mech.* **230**, 231–234.

Diebels, S., Schuster, B. & Hutter, K. 1994 Nonlinear internal waves over variable topography. *Geophys. Astrophys. Fluid Dyn.* **76**, 165–192.

Evans, W. A. B. & Ford, M. J. 1996 An integral equation approach to internal (2-layer) solitary waves. *Phys. Fluids* **8**, 2032–2047.

Farmer, D. M. 1978 Observations of long nonlinear waves in a lake. *J. Phys. Oceanogr.* **8**, 63–73.

Fu, L. L. & Holt, B. 1982 Internal waves in the gulf of California: observations from spaceborne radar. *J. Geophys. Res.* **89**, 2053–2060.

Funakoshi, M. 1985 Long internal waves in a two-layer fluid. *J. Phys. Soc. Japan* **54**, 2470–2476.

Funakoshi, M. & Oikawa, M. 1986 Long internal waves of large amplitude in a two-layer fluid. *J. Phys. Soc. Japan* **55**, 128–144.

Gerkema, T. & Zimmerman, J. T. F. 1994 Generation of nonlinear internal tides and solitary waves. *J. Phys. Oceanogr.* **25**, 1081–1094.

Goryachkin, Yu. N., Ivanov, V. A. & Pelinovsky, E. N. 1992 Transformation of internal tidal waves over the Guinean Shelf. *Sov. J. Phys. Oceanogr.* **3**, 309–315.

Halpern, D. 1971 Semidiurnal internal tides in Massachusetts Bay. *J. Geophys. Res.* **76**, 6573–6584.

Hammack, J. L. & Segur, H. 1974 The Korteweg-de Vries equation and water waves. Part 2. comparisons with experiments. *J. Fluid Mech.* **65**, 289–314.

Helfrich, K. R. & Melville, W. K. 1986 On long nonlinear internal waves over slope-shelf topography. *J. Fluid Mech.* **167**, 285–308.

Helfrich, K. R. & Melville, W. K. 1990 Review of dispersive and resonant effects in internal wave propagation. In *The Physical Oceanography of Sea Straits* (ed. L. J. Pratt), pp. 391–420.

Helfrich, K. R., Melville, W. K. & Miles, J. W. 1984 On interfacial solitary waves over slowly varying topography. *J. Fluid Mech.* **149**, 305–317.

Holyer, J. Y. 1979 Large amplitude progressive interfacial waves. *J. Fluid Mech.* **93**, 433–438.

Imberger, J. 1995 Flux path in a stratified lake: a review. *IUTAM Symp. on Physical Limnology, Broome, Western Australia*, pp. 423–439.

Kakutani, T. & Yamasaki, N. 1978 Solitary waves on a two-layer fluid. *J. Phys. Soc. Japan* **45**, 674–679.

Kao, T. W., Pan, F.-Sh. & Renouard, D. 1985 Internal solitons on the pycnocline: generation, propagation, and shoaling and breaking over a slope. *J. Fluid Mech.* **159**, 19–53.

Keulegan, G. H. 1953 Characteristics of internal solitary waves. *J. Res. Natl Bur. Stand.* **51**, 133–140.

Koop, C. G. & Butler, G. 1981 An investigation of internal solitary waves in a two-fluid system. *J. Fluid Mech.* **112**, 225–251.

Korteweg, D. J. & de Vries, G. 1895 On the change of form of long waves advancing in a rectangular canal, and on a new type of stationary waves. *Phil. Mag.* **39**, 422–443.

Kubota, T., Ko, D. R. S. & Dobbs, L. D. 1978 Propagation of weakly nonlinear internal waves in a stratified fluid of finite depth. *AIAA J. Hydronaut.* **12**, 157–165.

Kuznetsov, A. S., Paramonov, A. N. & Stepanyants, Y. A. 1984 Investigation of solitary internal waves in the tropical zone of West Atlantics. *Izv. Akad. Nauk SSSR: Fiz. Atmos. i Okeana* **20**(10), 975–984 (translated from Russian).

Lamb, K. G. 1994 Numerical experiments of internal wave generation by strong tidal flow across a finite amplitude bank edge. *J. Geophys. Res.* **99**, 843–864.

Lee, Ch.-Y. & Beardsley, R. C. 1974 The generation of long nonlinear internal waves in a weakly stratified shear flow. *J. Geophys. Res.* **79**, 453–462.

Leone, C., Segur, H. & Hammack, J. L. 1982 The viscous decay of long internal solitary waves. *Phys. Fluids* **25**, 942–944.

Long, R. R. 1956 Solitary waves in one- and two-fluid systems. *Tellus* **8**, 460–471.

Maurer, J., Hutter, K. & Diebels, S. 1996 Viscous effects in internal waves of two-layered fluids with variable depth. *Eur. J. Mech.* B/*Fluids* **15**, 445–470.

Mei, C. C. 1989 *The Applied Dynamics of Ocean Surface Waves* World Scientific.

Michallet, H. 1995 Etude théorique et expérimentale des ondes solitaires interfaciales. PhD thesis, Université Joseph Fourier, Grenoble.

MICHALLET, H. & BARTHÉLEMY, E. 1997 Ultrasonic probes and data processing to study interfacial solitary waves. *Exp. Fluids* **22**, 380–386.

MILES, J. W. 1979 On internal solitary waves. *Tellus* **31**, 456–462.

MILES, J. W. 1981 On internal solitary waves II. *Tellus* **33**, 397–401.

MIYATA, M. 1985 An internal solitary wave of large amplitude. *La Mer* **23**, 43–48.

MIYATA, M. 1988 Long internal waves of large amplitude. In *Nonlinear Water Waves* (ed. K. Horikawa & H. Maruo), pp. 399–406. Springer.

ONO, H. 1975 Algebraic solitary waves in statified fluids. *J. Phys. Soc. Japan* **39**, 1082.

OSTROVSKY, L. A. & STEPANYANTS, YU. A. 1989 Do internal solitons exist in the ocean? *Rev. Geophys.* **27**, 293–310.

PAN, F.-SH. 1984 Shoaling of internal solitary wave and interfacial instability. PhD thesis, School of Engineering and Architecture of the Catholic University of America, Washington.

RIENECKER, M. M. & FENTON, J. D. 1981 A Fourier approximation method for steady water waves. *J. Fluid Mech.* **104**, 119–137.

SANDSTROM, H. & ELLIOTT, J. A. 1984 Internal tide and solitons on the Scotian shelf: a nutrient pump at work. *J. Geophys. Res.* **89**, 6415–6426.

SEGUR, H. & HAMMACK, J. L. 1982 Soliton models of long internal waves. *J. Fluid Mech.* **118**, 285–304.

STEVENS, C., LAWRENCE, G., HAMBLIN, P. & CARMACK, E. 1996 Wind forcing of internal waves in a long narrow stratified lake. *Dyn. Atmos. Oceans* **24**, 41–50.

TURNER, R. E. L. & VANDEN-BROECK, J.-M. 1988 Broadening of interfacial solitary waves. *Phys. Fluids* **31**, 2486–2490.

WALKER, L. R. 1973 Interfacial solitary waves in a two fluid medium. *Phys. Fluids* **16**, 1796.

WATSON, G. & ROBINSON, I. S. 1991 A numerical model of internal wave refraction in the Strait of Gibraltar. *J. Phys. Oceanogr.* **21**, 185–204.

WESSELS, F. & HUTTER, K. 1996 Interaction of internal waves with a topographic sill in a two-layered fluid. *J. Phys. Oceanogr.* **26**, 5–20.